Control-Oriented Models for Ink-jet 3D Printing

Yijie Guo[1], Joost Peters[2], Tom Oomen[2], Sandipan Mishra[1]

Abstract

This paper proposes two control-oriented models to describe the layer-to-layer height evolution of the ink-jet 3D printing process. While the process has found wide applicability, as with many industrial 3D printing systems, ink-jet 3D printers operated in open loop, even when sensor measurements are available. One of the primary reasons for this is the lack of suitable control-oriented models of the process. To address this issue, two control-oriented models are proposed in this paper, the first is based on droplet geometry superposition, while the other is based on a graph-based characterization of local flow dynamics. The superposition model ignores the flow of the deposited liquid material, while the graph-based dynamic model is able to capture this phenomenon. These two models are compared with an existing flow-based empirical model and validated with experimental results, with the graph-based dynamic model demonstrating between 5-14 % improvement in layer height prediction. Both the superposition model and the graph-based dynamic model are suitable for closed-loop control algorithm design (as they are discrete layer-to-layer state-space models). We envision that these control-oriented models will ultimately enable the design of model-based closed-loop control for high resolution ink-jet 3D printing.

1. INTRODUCTION

Additive Manufacturing (AM) is a class of manufacturing processes in which material is added layer-upon-layer to construct three dimensional (3D) objects. Recently, AM has seen a significant increase in popularity for consumer, commercial and research [1] applications. The process under study in this manuscript is ink-jet 3D printing, which has been widely applied in commercial printers for its simplicity and small droplet size (10 to 500 μm), which enables high resolution printing.

Ink-jet 3D printers build 3D objects by jetting photopolymer layer-upon-layer with UV (ultra-violet) light curing in between. Currently, this process is typically performed in an open-loop manner, which implies that the number of layers to be deposited and the droplet patterns for each layer are determined in advance. This open-loop approach is vulnerable to uncertainties in droplet sizes, shapes, and locations since it does not use any feedback of the layer height profile during printing. This can result in undesired part geometry when the printed shape does not match the desired geometry [2].

One approach to dealing with uncertainties, disturbances and process drift is through closed-loop feedback control. There have been several studies on the closed-loop control of ink-jet 3D printing. However, most of them concentrate on the low-level closed-loop control of process variables, e.g., jetting frequency and droplet volume, as in [3, 4, 5]. Very limited work directly deals with geometry level closed-loop control [6, 7, 8], primarily because no appropriate control-oriented models are available that describe the layer-to-layer height evolution in the printing process sufficiently accurately. In the existing literature on modeling of ink-jet printing processes, several modeling approaches have been proposed, with varying levels of complexity and resolution. For the traditional 2D ink-jet printing process, ink channel dynamic models that describe the relationship between the waveform and the piezo sensor signal have been studied extensively to design the waveform to deposit droplets consistently and fast [9, 10, 11]. Although for 2D applications these models are useful, since in ink-jet 3D printing the droplet height is critical, these models are inadequate.

To address this, models describing the ink-jet 3D printing process have been developed. The so-called spherical lens model was proposed for a single droplet in [12, 13], while a numerical model describing the shape of liquid droplets deposited on a porous surface was proposed in [14]. Coalescence of droplets and the influence of droplet spacing on the morphology of a line of droplets was studied in [15, 16]. These models describe 3D geometries of a single droplet or a line of droplets. For direct modeling of the whole part geometry, a distributed parameter dynamic model was proposed in [12], which uses measurement of the measurable region to predict the geometry of the unmeasurable region. In [6, 2], a flow-based empirical model is proposed to describe the height evolution by assuming the height increase is caused by droplets on the considered location and its neighbors. A method to nonlinearly change these height increase parameters based on the prior height profile is proposed to address the flow of the deposited liquid material. Based on the 2D model proposed in [17], a superposition model in matrix form is proposed by the author to allow the use of efficient

Email addresses: guoy7@rpi.edu (Yijie Guo), j.peters.2@student.tue.nl (Joost Peters), T.A.E.Oomen@tue.nl (Tom Oomen), mishrs2@rpi.edu (Sandipan Mishra)

[1]Yijie Guo and Sandipan Mishra are with the Mechanical, Aerospace and Nuclear Engineering Department, Rensselaer Polytechnic Institute, Troy, NY 12180 USA

[2]Joost Peters and Tom Oomen are with the Department of Mechanical Engineering, Eindhoven University of Technology, 5600 MB Eindhoven, The Netherlands

optimization algorithms for model predictive control [7]. Further, the layer height increase is assumed to be the summation of the droplet shape at each location, however the influence of the prior height profile caused by material flow is ignored.

The models introduced above have addressed certain aspects of the ink-jet printing process. However, for direct geometry feedback control it is necessary to develop models that directly describe 3D geometries, as in [12, 6, 2, 7]. In [12], an algorithm is proposed to predict the geometry of the region under the printing nozzle, which cannot be measured by the 2D laser sensor during the printing process. In [6, 2], the effect of the prior height profile (i.e., the height profile of the previously deposited layers) on the current layer height and geometry is addressed based on a nonlinear flow function. A control-oriented model for 3D height evolution was proposed in [7]. The influence of the prior height profile was ignored in that study, although it resulted in an efficient control algorithm design strategy. For control of the ink-jet 3D process, we consider layer-to-layer control, which requires a layer-to-layer height evolution model, unlike the in-layer prediction model in [12]. Furthermore, we want the model to be suitable for control algorithm design, while retaining high fidelity. The nonlinear empirical model in [6, 2] and the low fidelity model in [7] cannot address both these needs simultaneously. Thus, The goal of this paper is to construct a control-oriented layer-to-layer height evolution model with high fidelity.

The key contributions of this paper are: (1). a graph-based dynamic layer-to-layer height evolution model that can capture the in-layer flow dynamics of the deposited liquid material and also is suitable for closed-loop control algorithm design; and (2). experimental verification and validation of this model, against the superposition model that the author proposed in [7] as well as the flow-based empirical model in [6, 2] by comparing their predictions with experimental results.

The paper is organized as follows. First, the ink-jet 3D printing process is described in Sec. 2 to provide a background for the model development. Next, in Sec. 3 the superposition model the author proposed in [7] is presented in more details as a basis for modeling the process. A graph-based dynamic model that captures the flow of the deposited material sufficiently accurately while being suitable for control algorithm design is proposed in Sec. 4. The flow-based empirical model proposed in [6, 2] is revisited in Sec. 5 for comparison. Finally, prediction results of the above three models are compared with experimental results in Sec. 6.

2. Ink-jet 3D Printing Process

Ink-jet 3D printing builds parts by jetting material from nozzles layer-upon-layer, with ultraviolet (UV) light curing between successive layers of deposition. There are three steps for printing one layer as shown in Fig. 1. First, nozzles deposit photopolymer ink on an existing layer at predetermined locations. Then, the printed layer in liquid state is cured by UV light. Finally, a laser sensor scans the finished layer and measures the height profile for feedback control. In our testbed, in the first ink-jet printing step, a single nozzle moves along a

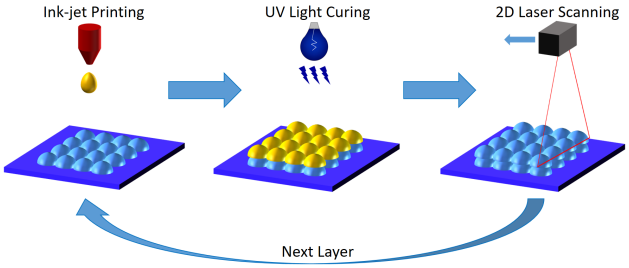

Figure 1: Three steps for printing one layer. First, nozzles deposit photopolymer ink on an existing layer at predetermined locations. Then, the printed layer in liquid state is cured to solid state by UV light. Finally, a 2D laser sensor scans the finished layer and gets height profile measurement for control.

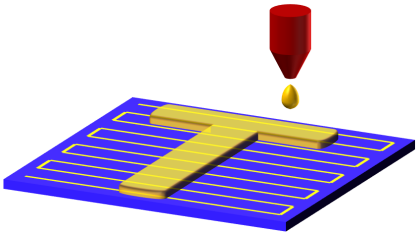

Figure 2: Printing process for one layer. A single nozzle (in our testbed) moves along a predetermined printing path and deposits droplets sequentially.

predetermined printing path and deposits droplets sequentially. Typically, the printing path is a raster path as shown in Fig. 2. We assume that the curing of the material is a chemical process that only marginally influences the volume of the printed shape. This means that the height profile evolution primarily occurs at the first step in Fig. 1, since the UV light curing step has minimal influence on the geometry shape.

In the following sections, we revisit existing control-oriented models and propose a new model to describe the height evolution. The print region is discretized into an $n_x \times n_y$ grid, the number of nodes in the grid is $n = n_x n_y$. Droplets are only deposited at nodes in the grid. We now present three models for capturing the height evolution based on the prior layer height and the droplet pattern to be deposited. We first describe a simple and intuitive superposition model that the authors proposed in [7] in the next section.

3. Superposition Model

In this section, a superposition model in a compact matrix form is presented. The central idea behind this model is that the layer height increase is the summation of droplet shape at each location as shown in Fig. 3. This assumption ignores the initial height profile's influence on the distribution of the deposited material caused by flow. However, the simple linear matrix form of the model makes it suitable for control algorithm design, especially for optimization-based control design strategies.

First, the droplet pattern $U_L \in R^{n_x \times n_y}$ and height profile $H_L \in R^{n_x \times n_y}$, as in Fig. 3, are rewritten into vectorized forms $\mathbf{u}_L \in R^n$

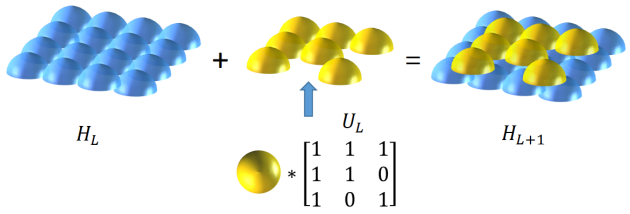

Figure 3: In the superposition model, the layer height increase is assumed to be the summation of droplet shape at each location, regardless of the prior layer height profile.

and $\mathbf{h}_L \in R^n$ (with L being the index for the layer number) as

$$U_L = \begin{bmatrix} U_L(1,1) & U_L(1,2) & \cdots & U_L(1,n_y) \\ U_L(2,1) & U_L(2,2) & \cdots & U_L(2,n_y) \\ \vdots & \vdots & \ddots & \vdots \\ U_L(n_x,1) & U_L(n_x,2) & \cdots & U_L(n_x,n_y) \end{bmatrix} \xrightarrow{\text{vectorize}} \begin{bmatrix} U_L(1,1) \\ U_L(1,2) \\ \vdots \\ U_L(1,n_y) \\ U_L(2,1) \\ \vdots \end{bmatrix} = u_L, \tag{1}$$

$$H_L = \begin{bmatrix} H_L(1,1) & H_L(1,2) & \cdots & H_L(1,n_y) \\ H_L(2,1) & H_L(2,2) & \cdots & H_L(2,n_y) \\ \vdots & \vdots & \ddots & \vdots \\ H_L(n_x,1) & H_L(n_x,2) & \cdots & H_L(n_x,n_y) \end{bmatrix} \xrightarrow{\text{vectorize}} \begin{bmatrix} H_L(1,1) \\ H_L(1,2) \\ \vdots \\ H_L(1,n_y) \\ H_L(2,1) \\ \vdots \end{bmatrix} = h_L. \tag{2}$$

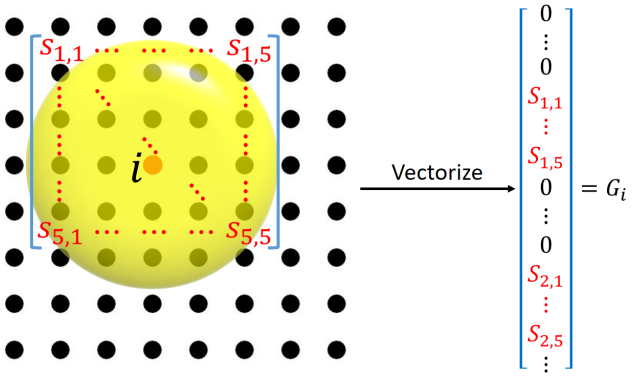

Figure 4: The droplet shape is captured by the matrix S, in this case, $S \in R^5$, $G_i \in R^{n\times 1}$ describes the height increase of each node in the whole printing region caused by the single droplet at the i^{th} node.

The droplet shape is captured by a matrix, whose size is determined by the grid resolution. For example, a 5×5 droplet shape is shown in Fig. 4. Based on the idea that the layer height increase is the summation of the droplet shape at each location, the layer-to-layer height evolution model can be written as:

$$h_{L+1} = h_L + \sum_{i=1}^{n} G_i u_L(i), \tag{3}$$

where G_i is a vector that represents the unit size droplet shape deposited at the i^{th} node in the grid as shown in Fig. 4. Each node inside the droplet area will have a certain height increase, while nodes outside of this area will not be influenced. The height increase at each node in the whole printing area caused by the single droplet at the i^{th} node is described by $G_i \in R^{n\times 1}$. The droplet volume at the i^{th} node is represented by $u_L(i)$.

The layer-to-layer height evolution model is then rewritten in a compact matrix form as below:

$$h_{L+1} = h_L + Gu_L, \tag{4}$$

where the $G \in R^{n\times n}$ with the i^{th} column being G_i. Although the influence of the prior height profile is ignored, this linear model is suitable for controller design and an optimization based feedback controller is designed in [7]. However, when compared with real data from experiments, this model does not capture material flow and spreading, especially at the edges. To capture this phenomenon, a novel graph-based dynamic model is proposed in the next section.

4. Graph-based Dynamic Model

In this section, a graph-based layer-to-layer height evolution model that can capture the flow of the deposited liquid material is proposed. This model is inspired by lumped heat transfer models, such as those used in building temperature control [18]. The key idea behind this model is that fluid flows from higher to lower height proportional to the height difference, as in heat transfer from higher to lower temperature.

As we introduced in Sec. 2, in the printing process, droplets are sequentially deposited along a predetermined printing path. At each time step in one layer printing, the nozzle moves to a certain location according to the printing path. The height change at node i at time step k is described by:

$$\Delta h_{i,k} = -\sum_{j\in\mathcal{N}_i} K_{ij}(h_{i,k} - h_{j,k}) + B_{i,k}u_k, \tag{5}$$

where $\mathcal{N}_i$ is the set of neighbors of node i. The first term $-\sum_{j\in\mathcal{N}_i} K_{i,j}(h_{i,k} - h_{j,k})$ captures the effect that the deposited liquid material will flow from higher to lower height, $K_{ij} > 0$ represents the flowability parameter that describes how much the liquid will flow based on neighbors' height difference. The second term $B_{i,k}u_k$ captures the material deposition, $B_{i,k}$ is the height increase at node i caused by unit size droplet at time step k as in Fig. 6, u_k is the droplet volume at time step k.

The incidence matrix D captures the connectivity (through links) between nodes in a directed graph. Fig. 7 is an example

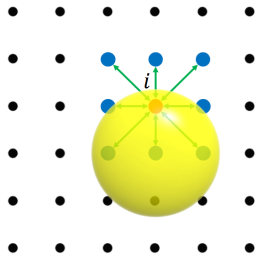

Figure 5: Node i's height change at time step k is caused by material flow between neighbors and the deposited droplet at time step k.

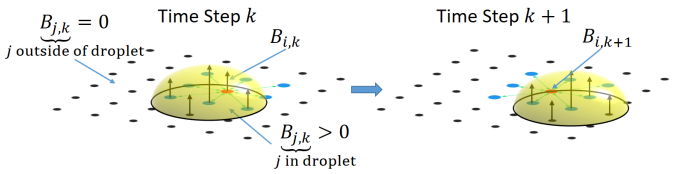

Figure 6: $B_{i,k}$ is the height increase at node i caused by a unit-size droplet at time step k, all nodes' height increase caused by this unit-size droplet creates the $n \times 1$ vector B_k. If node j is in the droplet, $B_{j,k} > 0$, if node j is outside of the droplet's region of impact, $B_{j,k} = 0$. Note that B_k is updated with each time step, as the droplet deposition location will change at each time step.

of a directed graph. The elements of D are defined by

$$D(p,q) = \begin{cases} 1, & \text{if link } q \text{ ends at node } p \\ -1, & \text{if link } q \text{ starts at node } p \\ 0, & \text{otherwise.} \end{cases} \tag{6}$$

This allows us to combine (5) and (6) into (7), where the height evolution model at time step k is described as:

$$h_{k+1} = h_k - DK_kD^Th_k + B_ku_k, \tag{7}$$

where $h_k \in \mathbb{R}^n$ is a column vector that defines the height of the layer when the nozzle is at time step k in the printing path, $D \in \mathbb{R}^{n\times l}$, with l the number of links, is the incidence matrix. Diagonal positive definite matrix $K \in \mathbb{R}^{l\times l}$ contains the flowability parameters. Here, K_k is updated with each time step to set the active links that are influenced by the flow dynamics. Fig.

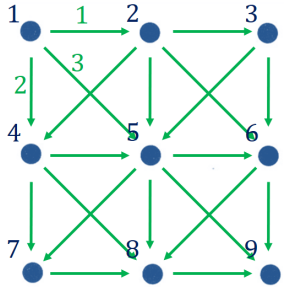

Figure 7: Example of a directed graph for a 3×3 grid. Incidence matrix D describes the relationship between links and nodes. According to (6), $D(1,1) = -1$ because link 1 starts at node 1, $D(2,1) = 1$ because link 1 ends at node 2.

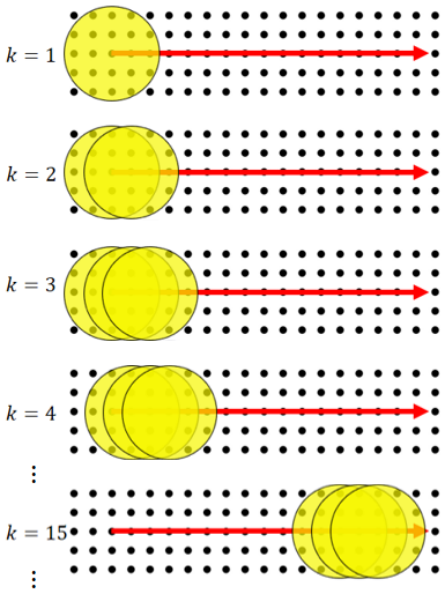

Figure 8: Flow dynamics are localized to where new material is deposited and last only for a limited period of time (termed flow duration). Thus, as the nozzle moves along the printing path and deposits material sequentially, the active flow dynamics region is updated with time. The figure above is an illustration of the mechanism for active region update with flow duration time being 3 time steps, where k indicates time step. The red arrow is the printing path and the yellow circles represent active regions.

8 shows how the flow dynamics active region is updated with each time step. Only links inside the active region is set active in the model. Unit size droplet shape and location are contained in the column vector $B_k \in \mathbb{R}^n$. For example, at time step k, the droplet shape is shown as the spherical cap in Fig. 6. All the nodes' height increase in the grid caused by this droplet constructs a $n \times 1$ vector B_k, if node j is in the droplet, $B_{j,k} > 0$, if node j is outside of the droplet, $B_{j,k} = 0$.

Layer Evolution Model

The model described in the previous section captures the height evolution from *time step* to *time step*. We now present a layer-to-layer model derived from this model through lifting from time-domain to layer-domain. First, the time step height evolution model (7) is rewritten as

$$h_{k+1} = A_kh_k + B_ku_k, \tag{8}$$

where $A_k = (I - DK_kD^T)$, $k \in \{1, 2..n\}$. At the final time step n of printing one layer, the height profile can be calculated as:

$$h_n = (\prod_{i=n}^{1} A_i)h_1 + \begin{bmatrix} (\prod_{i=n}^{2} A_i)B_1 \\ (\prod_{i=n}^{3} A_i)B_2 \\ \vdots \\ A_nB_{n-1} \\ B_n \end{bmatrix}^T \begin{bmatrix} u_1 \\ u_2 \\ \vdots \\ u_{n-1} \\ u_n \end{bmatrix}, \tag{9}$$

Assume we are printing the $(L+1)^{th}$ layer, the first time step height profile h_1 is actually h_L, the final height profile of the L^{th}

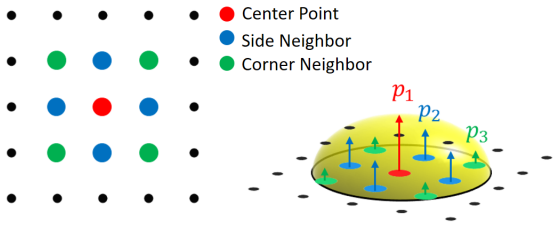

Figure 9: Based on the relative location to the droplet center, the grid points are categorized into three types: center point, side neighbor and corner neighbor. The height changes of these three types of points caused by depositing one droplet on the center point are denoted as p_1, p_2, p_3.

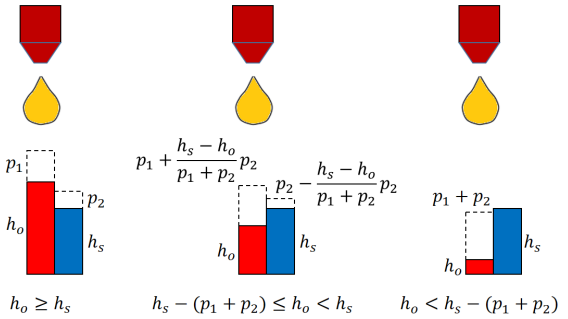

Figure 10: Height changes at the center points and one of its side neighbors vary depending on their previous layer height h_o and h_s.

layer printing, the final time step height profile h_n is actually h_{L+1}, the final height profile of the $(L+1)^{th}$ layer printing. From now on, h_L will only represent the layer height profile, the time step hight profile notation h_k will be disused. Then, we can have our layer-to-layer height evolution model (with L as the layer number):

$$h_{L+1} = \mathcal{A}h_L + \mathcal{B}u_L, \tag{10}$$

where $\mathcal{A} \in \mathbb{R}^{n\times n}$ is $\prod_{i=n}^{1} A_i$, $\mathcal{B} \in \mathbb{R}^{n\times n}$ is

$$\begin{bmatrix} (\prod_{i=n}^{2} A_i)B_1 & (\prod_{i=n}^{3} A_i)B_2 & \cdots & A_nB_{n-1} & B_n \end{bmatrix},$$

the L^{th} layer control input u_L is

$$\begin{bmatrix} u_1 & u_2 & \cdots & u_{n-1} & u_n \end{bmatrix}^T,$$

where the k^{th} element in u_L is the k^{th} time step's control input when printing this layer. If the nozzle moves along a certain path, then $\mathcal{A}$, $\mathcal{B}$ are fixed for each layer.

Thus, we now have a layer-to-layer model that accounts for the flow of the material during the printing process. With this lifted description of the linear time-invariant layer-to-layer height evolution model, a closed-loop control algorithm can be conveniently designed. Before we experimentally compare and evaluate the proposed model with existing models, a flow-based empirical model from [2] is presented.

5. Flow-based Empirical Model

The flow-based empirical model proposed by Lu et al [6, 2] is revisited in this section. It assumes that the height change at each point is resulted from droplets deposited at this point and its eight neighbors. Based on the relative location to the considered point, the grid points are categorized into three types: center point, side neighbor and corner neighbor, as shown in Fig. 9. The height changes at these three locations caused by depositing one droplet on the center point are denoted as p_1, p_2, p_3 respectively. These parameters are identified by measuring deposited droplets on flat surface.

In order to take into account the influence of the prior height profile caused by material flow, p_1, p_2, p_3 are modified based on the height differences between neighbors. Take the side neighbors for example. Fig. 10 shows how the height changes at the center point and one of its side neighbors vary depending on their height difference on the previous layer. If the previous height at center h_o is greater than or equal to that of the side neighbor h_s, p_1 and p_2 stay the same. If $h_o < h_s$, the fluid is constrained inside the center and the height change at the side neighbor will be reduced. The constrained volume is proportional to $h_s - h_o$ until $h_o = h_s - (p_1 + p_2)$. From then on, the height change at the center point is always $p_1 + p_2$. The corner neighbors' height increase is modified using the same method. This flow process is captured by the flow back function Eq. (15).

Then the height change of point (i, j) is given by

$$\Delta H(i, j) = P_1(i, j) + P_2(i, j) + P_3(i, j). \tag{11}$$

where $P_1(i, j)$ is the height change resulted from the droplet deposited at point (i, j), $P_2(i, j)$ is the height change resulted from the droplets deposited at four side neighbors of point (i, j), $P_3(i, j)$ is the height change resulted from the droplets deposited at four corner neighbors of point (i, j).

The terms P_1, P_2 and P_3 are formulated as follows:

$$\begin{aligned} P_1 \quad &= U(i, j)(p_1 + p_2 \sum_{(m,n)\in\mathcal{S}(i,j)} f(p_1 + p_2, H_k(i, j) - H_k(m, n)) \\ &\quad + p_3 \sum_{(m,n)\in\mathcal{C}(i,j)} f(p_1 + p_3, H(i, j) - H(m, n))), \end{aligned} \tag{12}$$

$$P_2 = p_2 \sum_{(m,n)\in\mathcal{S}(i,j)} U(m, n)(1 - f(p_1 + p_2, H(m, n) - H(i, j))), \tag{13}$$

$$P_3 = p_3 \sum_{(m,n)\in\mathcal{C}(i,j)} U(m, n)(1 - f(p_1 + p_3, H(m, n) - H(i, j))), \tag{14}$$

where $U(i, j)$ is the droplet volume deposited at point (i, j). The set of side neighbors of point (i, j) is noted by $\mathcal{S}(i, j)$. The set of corner neighbors of point (i, j) is noted by $\mathcal{C}(i, j)$.

The flow back function $f(a, b)$ characterizes how material flow in terms of the height difference between two points, and is defined by

$$f(a, b) = \begin{cases} 0, & \text{if } b \geq 0, \\ -\frac{b}{a}, & \text{if } -a \leq b < 0, \\ 1, & \text{else.} \end{cases} \tag{15}$$

This empirical model takes into account the prior height's influence on the distribution of the deposited material, but in order to predict the height evolution of a layer, every point's height

needs to calculated using the nonlinear function (15), which makes the closed-loop control algorithm design difficult.

6. EXPERIMENTAL RESULTS

In this section, the predicted height profiles using the three models discussed above are compared with experimental results. Three printing experiments are implemented: printing an $8mm \times 8mm$ square with 12 layers, printing a $10mm \times 10mm$ 'E' shape with 12 layers and printing an $8mm \times 8mm$ square with 12 layers on an uneven base with an 'E' shape.

6.1. Printing Strategy

Based on the resolution of the laser scanner, the grid spacing is chosen as $0.125mm$. For a better surface finish, the line spacing (space between droplets) is chosen as two grid spaces ($0.25mm$). Thus, not all the points in the grid are printed in one layer, instead of printing on the same grid points each layer, alternate grid points are printed in successive layers. Fig. 11 illustrates these grid points for successive layers. For this case, line spacing is twice the grid size and thus we need 4 layers to print all the points in the gird. For larger line spacing, we may follow the same procedure. Using this printing strategy, we can achieve a more even top surface.

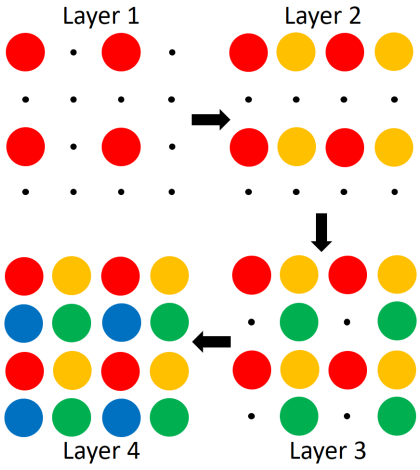

Figure 11: Different grid points are printed between successive layers, line spacing is twice of the grid size in our printing and 4 layers are needed to print all the points in the grid.

6.2. Experimental Verification

To use the proposed models for prediction of the printed height profile, we first need to identify the droplet shape that is necessary for all three models and for the graph-based dynamic model we must also determine the flowability parameter. In this section, an $8mm \times 8mm$ square is first printed to identify these parameters and verify the model.

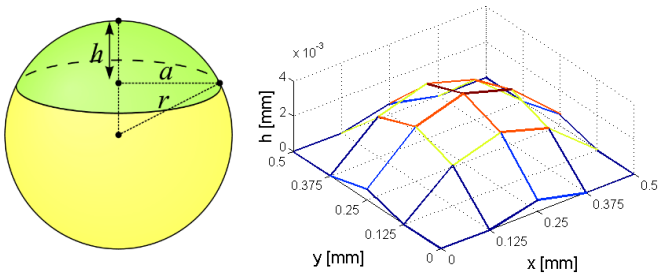

Figure 12: Droplet shape can be modeled as a spherical lens, the discretized droplet shape used in all three models is shown on the right.

6.2.1. Identification of Droplet Shape

Because of the small size of the droplet (radius is about $500\mu m$ and peak height is about 4 μm) and its transparency, droplet shape is difficult to measure directly using the laser scanner or an optical microscope, hence a spherical lens model is used to estimate its shape.

The shape of a droplet on an even surface can be modeled as a spherical lens [12] as shown in Fig. 12. The volume V of the droplet shape is calculated as:

$$V = \pi h/6(3a^2 + h^2). \tag{16}$$

Though it is difficult to directly measure the droplet shape, the average volume V of one droplet can be calculated by dividing the volume of the printed square as shown in Fig. 13 by the number of deposited droplets. The base radius a can also be measured using an optical microscope. Thus, with V and a, Eq. (16) is solved for h and thus the droplet shape is obtained. The discretized droplet shape obtained using this method is shown in Fig.12 (right).

6.2.2. Identification of Flowability Parameter

After determining the droplet shape, the flowabilty parameters $K_{i,j}$ in Eq. (5) need to be identified. Since the printing surface is assumed to be homogeneous and isotropic, it is reasonable to assume that $K_{i,j} = k_{flow}\ \forall i,\ j$. After obtaining the measured height profile of the printed square H_{ex}, k_{flow} is identified by solving

$$k_{flow} = \arg\min_{k_{flow}} \left\| H_{ex} - H_{sim}(k_{flow}) \right\|_2, \tag{17}$$

This problem has only one optimization parameter, however calculation of the gradient of the cost with respect to this single parameter is difficult, thus a golden search method is used to solve for the optimal flowabilty parameter value. The optimal value obtained through golden search is $k_{flow} = 0.031$.

Finally, after obtaining the droplet shape and flowability parameter, the simulated height profiles using the three models are compared with the experimental result. The comparison is shown in Figure. 13, the height profiles shown in the figure are the final height profiles subtracted by the base height profiles (note that the flow-based empirical model's resolution is constrained to the line spacing, thus we use interpolation to com-

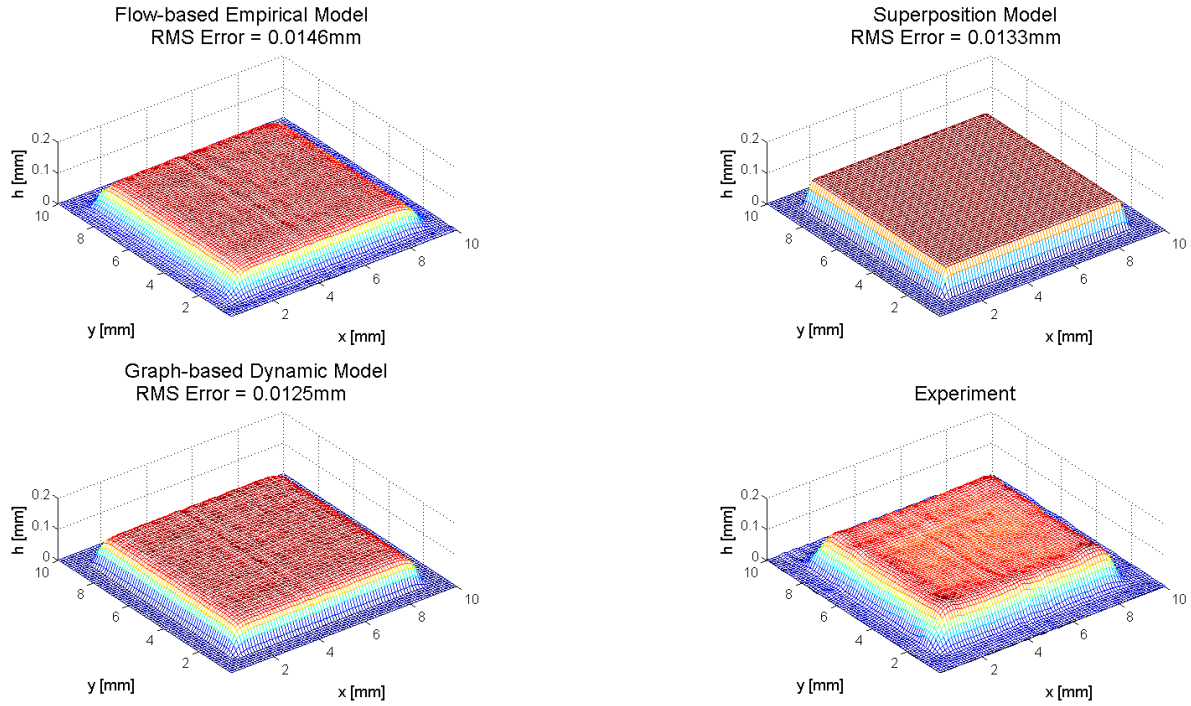

Figure 13: Comparison of the predicted height profiles using the three models and the experimental measurement from printing an $8mm \times 8mm$ square for 12 layers. Both the flow-based empirical model and the graph-based dynamic model can capture the influence of prior height profile and round edges caused by material flow. The graph-based dynamic model has the smallest RMS error. It demonstrates 6-14 % improvement in accuracy compared to the other two models.

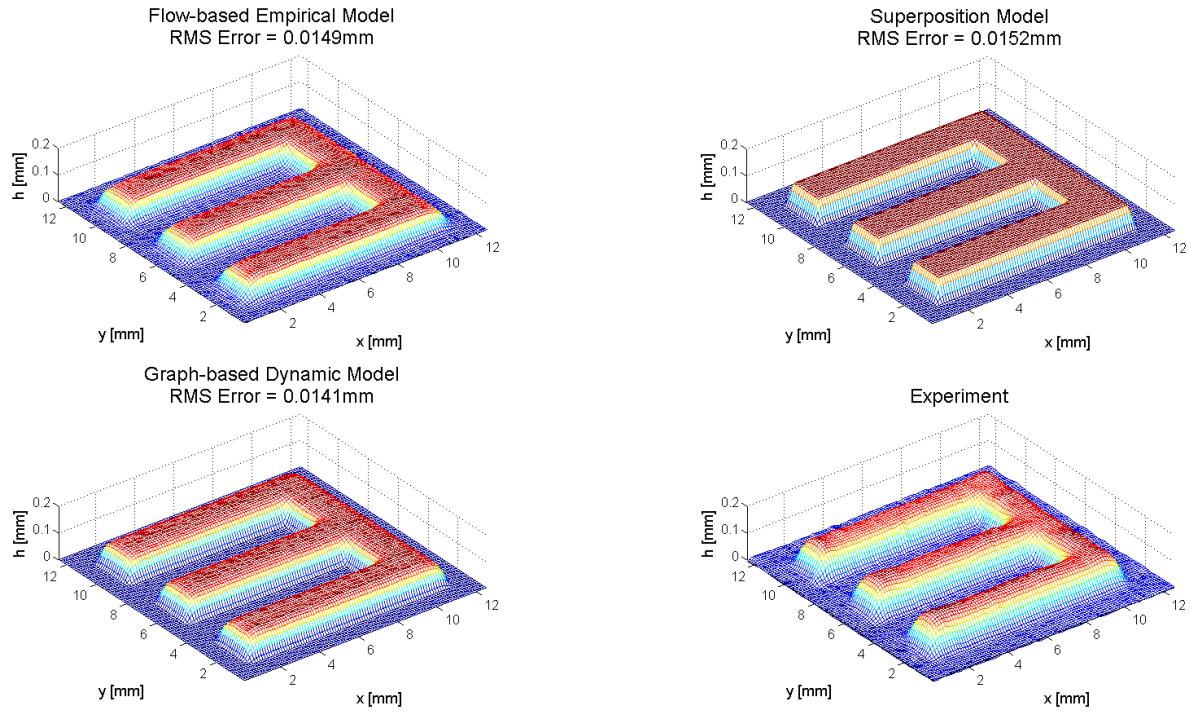

Figure 14: Comparison of the predicted height profiles using the three models and experimental measurements from printing a $10mm \times 10mm$ 'E' shape for 12 layers. Both the flow-based empirical model and the graph-based dynamic model can capture the round edges caused by material flow. The graph-based dynamic model has the smallest RMS error and demonstrates 5-8 % improvement in prediction accuracy compared with the other two models.

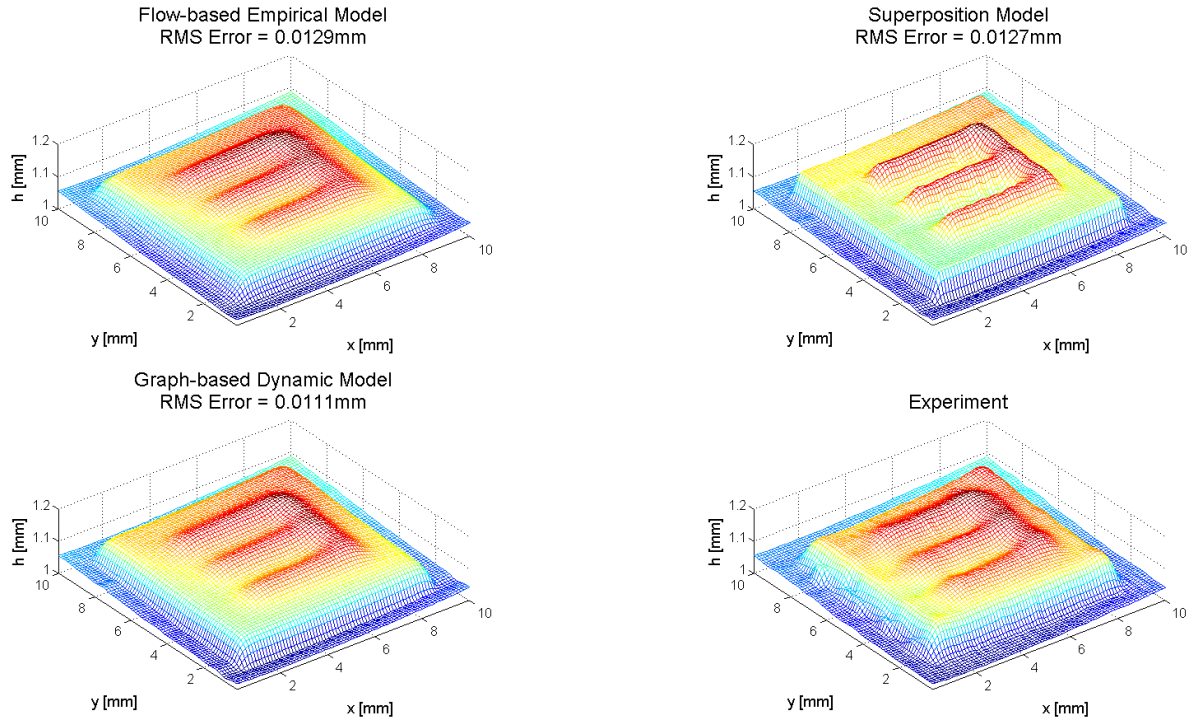

Figure 15: Comparison of the predicted height profiles using the three models and the experimental measurement from printing an $8mm \times 8mm$ square for 12 layers on an uneven base with an 'E' shape. Both the flow-based empirical model and the graph-based dynamic model can capture the influence of prior height profile and round edges caused by material flow. The graph-based dynamic model has the smallest RMS error and shows 13-14 % improvement in accuracy compared to the other two models.

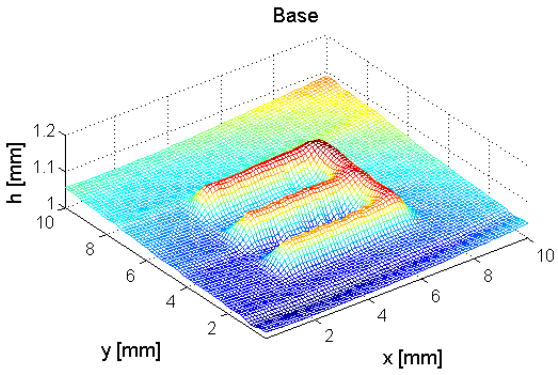

Figure 16: Uneven base with an 'E' shape.

pare it against the other two models.). Bases are fairly smooth with some textural variation. It is observed that both the flow-based empirical model and the graph-based dynamic model can capture the influence of these small textures, i.e, these two models can capture the prior height profile's influence. Furthermore, these two models can also capture the round edges caused by material flow, while the superposition model cannot capture either of these observed phenomena. By inspection of the root mean square error compared with the experimental result, it is observed that the graph-based dynamic model has the smallest error $0.0125mm$. It has 14 % and 6 % improvement in accuracy compared to the flow-based empirical model and the superposition model respectively. It's surprising that the flow-based empirical model has the largest error $0.0146mm$. This is caused by the over spreading at edges, because the empirical model's spreading is not identified from experiments but from an empirical function.

6.3. Experimental Validation

In this section, with the previous identified droplet shape and flowability parameter, these three models are used to predict the height profiles of two different printing cases, then their results are compared with real experimental results.

The first case is printing a $10mm \times 10mm$ 'E' shape for 12 layers. The predicted height profiles using the three models and the experimental result are shown in Fig. 14, it is observed that both the flow-based empirical model and the graph-based dynamic model can capture the round edges caused by material

flow, while the superposition model can not capture this. In terms of the root mean square error compared with the experimental result, the graph-based dynamic model has the smallest error $0.0141mm$. It has 5 % and 8 % improvement in accuracy compared to the flow-based empirical model and superposition model respectively.

The second case is printing an $8mm \times 8mm$ square for 12 layers on an uneven base as shown in Fig. 16. The predicted height profiles using the three models and the experimental result are shown in Fig. 15, it is observed that both the flow-based empirical model and the graph-based dynamic model can capture the round edges and the influence of the uneven base caused by material flow, while the superposition model can capture neither of them. In terms of the root mean square error compared with the experimental result, the graph-based dynamic model has the smallest error $0.0111mm$. It has 14 % and 13 % improvement in accuracy compared to the flow-based empirical model and the superposition model respectively.

In summary, both the graph-based dynamic model and the flow-based empirical model can capture the round edges and the influence of prior height profile caused by material flow, but the graph-based dynamic model can capture this more accurately though it is linear, because the flowability parameter is identified from experiments while the nonlinear flow-based empirical model uses an empirical flow back function to capture the flow. The superposition model can not capture the flow. In terms of root mean square error, the graph-based dynamic model always has the smallest error and has 5-14 % improvement in accuracy compared to the other two models.

7. CONCLUSION

In this manuscript, two control-oriented models are proposed to describe the layer-to-layer height evolution of the ink-jet 3D printing process. Both models are linear while the graph-based dynamic model can capture the material flow while the superposition model can not. These two models and an existing flow-based empirical model are compared with experimental results. Both the graph-based dynamic model and the flow-based empirical model can capture the round edges and the influence of the initial height profile, the graph-based dynamic model always has the smallest root mean square error and has 5-14 % improvement in accuracy compared to the other two models. In addition, the linearity of the graph-based dynamic model makes it suitable for closed-loop control algorithm design, future work will be the design and experimental implementation of the closed-loop control algorithm based on the graph-based dynamic model.

ACKNOWLEDGMENT

This work was supported in part by the National Science Foundation Career Award grant CMMI-1254313 and in part by the Center for Automation Technologies and Systems (CATS) under a block grant from the New York State Empire State Development Division of Science, Technology and Innovation (NYSTAR).

References

[1] S. L. Ford, Additive manufacturing technology: Potential implications for US manufacturing competitiveness, Journal of International Commerce and Economics .

[2] L. Lu, J. Zheng, S. Mishra, A Layer-To-Layer Model and Feedback Control of Ink-Jet 3-D Printing, IEEE/ASME Transactions on Mechatronics 20 (3).

[3] K. Barton, S. Mishra, A. Alleyne, P. Ferreira, J. Rogers, Control of high-resolution electrohydrodynamic jet printing, Control Engineering Practice 19 (11) (2011) 1266–1273.

[4] P. Ben-Tzvi, R. B. Mrad, A. A. Goldenberg, A conceptual design and FE analysis of a piezoceramic actuated dispensing system for microdrops generation in microarray applications, Mechatronics 17 (1) (2007) 1–13.

[5] W. Rone, P. Ben-Tzvi, Design and FE analysis of integrated sensing using gas compressibility for microdroplet generation, Mechatronics 23 (4) (2013) 397–408.

[6] L. Lu, J. Zheng, S. Mishra, A model-based layer-to-layer control algorithm for ink-jet 3d printing, in: Dynamic Systems and Control Conference (DSCC), 2014, ASME, V002T35A001–V002T35A001, 2014.

[7] Y. Guo, S. Mishra, A predictive control algorithm for layer-to-layer ink-jet 3D printing, in: American Control Conference (ACC), 2016, IEEE, 833–838, 2016.

[8] Y. Guo, J. Peters, T. Oomen, S. Mishra, Distributed Model Predictive Control for Ink-Jet 3D Printing, in: Advanced Intelligent Mechatronics (AIM), 2017 IEEE International Conference on, IEEE, 2017.

[9] M. G. Wassink, N. Bosch, O. Bosgra, S. Koekebakker, Enabling higher jet frequencies for an inkjet printhead using Iterative Learning Control, in: Control Applications, 2005. CCA 2005. Proceedings of 2005 IEEE Conference on, IEEE, 791–796, 2005.

[10] K.-S. Kwon, W. Kim, A waveform design method for high-speed inkjet printing based on self-sensing measurement, Sensors and Actuators A: Physical 140 (1) (2007) 75–83.

[11] A. A. Khalate, X. Bombois, R. Babuška, H. Wijshoff, R. Waarsing, Performance improvement of a drop-on-demand inkjet printhead using an optimization-based feedforward control method, Control Engineering Practice 19 (8) (2011) 771–781.

[12] C. Doumanidis, E. Skordeli, Distributed-parameter modeling for geometry control of manufacturing processes with material deposition, Journal of dynamic systems, measurement, and control 122 (1) (2000) 71–77.

[13] D. L. Cohen, H. Lipson, Geometric feedback control of discrete-deposition sff systems, Rapid Prototyping Journal 16 (5) (2010) 377–393.

[14] N. C. Reis, R. F. Griffiths, J. M. Santos, Numerical simulation of the impact of liquid droplets on porous surfaces, Journal of Computational Physics 198 (2) (2004) 747–770.

[15] D. Soltman, V. Subramanian, Inkjet-printed line morphologies and temperature control of the coffee ring effect, Langmuir 24 (5) (2008) 2224–2231.

[16] W. Lee, G. Son, Numerical study of droplet impact and coalescence in a microline patterning process, Computers & Fluids 42 (1) (2011) 26–36.

[17] D. J. Hoelzle, K. L. Barton, A new spatial Iterative Learning Control approach for improved micro-Additive Manufacturing, in: American Control Conference (ACC), 2014, IEEE, 1805–1810, 2014.

[18] H. Boyer, J. P. Chabriat, B. Grondin-Perez, C. Tourrand, J. Brau, Thermal building simulation and computer generation of nodal models, Building and environment 31 (3) (1996) 207–214.